6736 *Chem. Mater.* **2010,** *22,* 6736–6741
DOI:10.1021/cm102788b

CHEMISTRY OF MATERIALS
Article

Multicolor Conjugate Polyelectrolyte/Peptide Complexes as Self-Assembled Nanoparticles for Receptor-Targeted Cellular Imaging

Kan-Yi Pu,[†] Kai Li,[†] and Bin Liu*

Department of Chemical and Biomolecular Engineering, 4 Engineering Drive 4, National University of Singapore, Singapore 117576, Singapore. [†]Both authors contributed equally to this work

Received September 28, 2010. Revised Manuscript Received November 10, 2010

An anionic conjugated polyelectrolyte (CPE, **P1**) with energy donor−acceptor architecture is synthesized and assembled with an Arg-Gly-Asp (RGD) terminated peptide to form fluorescent nanoparticles (FNs) with targeting capability. Complexation between oppositely charged **P1** and the peptide at different molar ratio results in FNs with different size and fluorescence varying from sky-blue to orange-red because of aggregation-enhanced fluorescence resonance energy transfer (FRET). At the **P1**/peptide molar ratio of 8:0.9, the FNs exhibit bright orange-red fluorescence with a quantum yield of 16% and a large Stokes shift of 195 nm. In addition, these FNs also possess low cytotoxicity and good photostability. By virtue of the specific binding between RGD and integrin receptors, the **P1**/peptide FNs serve as an effective probe for receptor-targeted fluorescence imaging of HT29 cancer cells. This study thus provides a facile and generic strategy to prepare a new generation of multicolor polymeric FNs with native targeting capability and controllable properties for biological applications.

Introduction

Fluorescent nanoparticles (FNs) with molecular imaging functionality are of central significance not only for fundamental biology and pathophysiology but also for clinical diagnosis and therapy.[1] Although quantum dots (QDs) as inorganic FNs have been widely applied for biological sensing and imaging, their intrinsically toxic metallic ingredients render them potentially cytotoxic, consequently limiting their clinical applications.[2] In contrast, organic FNs possess better biocompatibility and higher versatility in composition.[3] However, they are usually generated from polymeric vesicles or micelles embedded with small-molecule chromophores, which inevitably share the intrinsic drawbacks of chromophores including fast photobleaching and small Stokes shift.[4] In addition, realization of targeting capability for current FNs generally requires complicated and laborious surface modification, which has a negative impact on their dimension and fluorescence properties.[4b] As a result, FNs born with targeting capability as well as good biophysical and optical properties remain to be explored.

Conjugated polyelectrolytes (CPEs) are fluorescent macromolecules with π-electron delocalized backbones and water-soluble ionic side chains.[5] With distinguished advantages over traditional small chromophores including large absorption extinction coefficient and efficient intramolecular/intermolecular exciton migration, CPEs provide a unique platform for the construction of organic light-emitting diodes,[6] solar cells,[7] and biosensors.[8] Recently, they have also been applied as nonspecific stains

*To whom correspondence should be addressed. Fax: (+65) 6779-1936. E-mail: cheliub@nus.edu.sg.

(1) (a) Jaiswal, J. K.; Mattoussi, H.; Mauro, J. M.; Simon, S. M. *Nat. Biotechnol.* **2003**, *21*, 47–51. (b) Lichtman, J. W.; Conchello, J. A. *Nat. Methods* **2005**, *2*, 910–919. (c) Michalet, X.; Pinaud, F. F.; Bentolila, L. A.; Tsay, J. M.; Doose, S.; Li, J. J.; Sundaresan, G.; Wu, A. M.; Gambhir, S. S.; Weiss, S. *Science* **2005**, *307*, 538–544. (d) Medintz, I. L.; Uyede, H. T.; Goldman, E. R.; Mattoussi, H. *Nat. Mater.* **2005**, *4*, 435–446. (e) Jin, Y.; Gao, X. *Nat. Nanotechnol.* **2009**, *4*, 571–576. (f) Hu, M.; Yan, J.; He, Y.; Lu, H. T.; Weng, L. X.; Song, S. P.; Fan, C. H.; Wang, L. H. *ACS Nano* **2010**, *4*, 488–494.

(2) (a) Derfus, A. M.; Chan, W. C. W.; Bhatia, S. N. *Nano Lett.* **2004**, *4*, 11–18. (b) Lichtman, J. W.; Conchello, J. A. *Nat. Methods* **2005**, *2*, 910–919. (c) Ryman-Rasmussen, J. P.; Riviere, J. E.; Monteiro-Riviere, N. A. *Nano Lett.* **2007**, *7*, 1344–1348. (d) Lee, J. S.; Mahendra, S.; Alvarez, P. J. J. *ACS Nano* **2010**, *4*, 3580–3590.

(3) (a) Torchilin, V. P. *J. Controlled Release* **2001**, *73*, 137–172. (b) Hawker, C. J.; Wooley, K. L. *Science* **2005**, *309*, 1200–1205. (c) Duncan, R. *Nat. Rev. Cancer* **2006**, *6*, 688–701.

(4) (a) Kirchner, C.; Liedl, T.; Kudera, S.; Pellegrino, T.; Javier, A. M.; Gaub, H. E.; Stolzle, S.; Fertig, N.; Parak, W. J. *Nano Lett.* **2005**, *5*, 331–338. (b) Resch-Genger, U.; Grabolle, M.; Cavaliere-Jaricot, S.; Nitschke, R.; Nann, T. *Nat. Methods* **2008**, *5*, 763–775.

(5) (a) Liu, B.; Bazan, G. C. *Chem. Mater.* **2004**, *16*, 4467–4476. (b) Thomas, S. W., III; Joly, G. D.; Swager, T. M. *Chem. Rev.* **2007**, *107*, 1339–1386. (c) Ho, H. A.; Najari, A.; Leclerc, M. *Acc. Chem. Res.* **2008**, *41*, 168–178. (d) Pu, K. Y.; Liu, B. *Biosens. Bioelectron.* **2009**, *24*, 1067–1073. (e) Jiang, H.; Taranekar, P.; Reynolds, J. R.; Schanze, K. *Angew. Chem., Int. Ed.* **2009**, *48*, 4300–4316. (f) Li, K.; Liu, B. *Polym. Chem.* **2010**, *1*, 252–259. (g) Duarte, A.; Pu, K. Y.; Liu, B.; Bazan, G. C. *Chem. Mater.* **2010**, DOI: 10.1021/cm102196t

(6) Hoven, C. V.; Garcia, A.; Bazan, G. C.; Nguyen, T. Q. *Adv. Mater.* **2008**, *20*, 3793–3810.

(7) (a) Taranekar, P.; Qiao, Q.; Jiang, H.; Ghiviriga, I.; Schanze, K. S.; Reynolds, J. R. *J. Am. Chem. Soc.* **2007**, *129*, 8958–8959. (b) Liu, X.; Zhu, R.; Yu, D.; Zhang, Y.; Liu, B.; Ramakrishna, S. *Chem. Commun.* **2008**, 3789–3791. (c) Huang, F.; Wu, H. B.; Cao, Y. *Chem. Soc. Rev.* **2010**, *39*, 2500–2521.

(8) (a) Chen, L.; McBranch, D. W.; Wang, H. L.; Helgeson, R.; Wudl, F.; Whitten, D. G. *Proc. Natl. Acad. Sci. U.S.A.* **1999**, *96*, 12287–12292. (b) Wang, D.; Gong, X.; Heeger, P. S.; Rininsland, F.; Bazan, G. C.; Heeger, A. J. *Proc. Natl. Acad. Sci. U.S.A.* **2002**, *109*, 49–53. (c) Pinto, M. R.; Schanze, K. S. *Proc. Natl. Acad. Sci. U.S.A.* **2004**, *101*, 7505–7510.

Published on Web 11/24/2010

for cellular imaging.[9] Primary studies reveal that CPEs have low cytotoxicity, good photostability, and sufficient brightness, paving the way for further exploration of their applications as a new generation of FNs. However, CPE-based FNs born wih targeting capability have not been reported to date.

Investigation on gene delivery has revealed that electrostatic attraction between deoxyribonucleic acid (DNA) and cationic polyelectrolyte plays a vital role in the formation of stable nanoparticles for cellular uptake.[10] This inspires us that FNs with native targeting capability could be prepared in a similar manner by replacing DNA with charged biorecognition molecules. However, the currently available CPEs generally have small Stokes shifts and undergo substantial fluorescence quenching upon aggregation or complexation with oppositely charged biomolecules.[11] These optical limitations make most CPEs not ideal for preparation of FNs via the complexation-mediated method.

Fluorescence resonance energy transfer (FRET) is a well-known photophysical process whereby different chromophores communicate their electronic states, providing means for transferring excitons from a donor to an acceptor.[12] On the basis that three-dimensional interchain energy transfer could be more efficient than one-dimensional intrachain transfer,[13] we have developed a series of multicolor CPEs with energy donor−acceptor backbones to exhibit aggregation-enhanced FRET.[14] When aggregation occurs, these CPEs emit intensified acceptor emission at long-wavelength region upon excitation at the donor moieties, which not only produce a large apparent Stoke shift but also preserve bright fluorescence. As a result, CPEs with donor−acceptor backbones are promising building blocks to form FNs with a biorecognition element for cellular imaging.

Scheme 1. Schematic Illustration of CPE/Peptide Nanoparticle Formation[a]

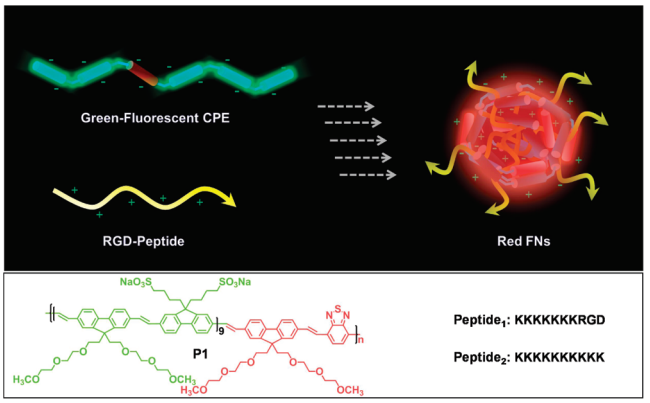

[a] The chemical structure of **P1** and the sequences of peptides are also shown in the scheme.

In this contribution, we report multicolor CPE-based polymeric FNs with native targeting capability, high photostability, and large Stokes shift for cellular imaging. As depicted in Scheme 1, the FNs are self-assembled from electrostatic-interaction-induced complexation between an anionic CPE (**P1**) and a cationic peptide. The backbone of **P1** is based on polyfluorenyldivinylene (PFV) incorporated with 5 mol % benzothiadiazole (BT), which allows for efficient energy transfer from the PFV fragments to the BT units upon nanoparticle formation. In addition, **P1** is designed to have oligo(ethylene oxide) (OEO) side chains, which endow the formed FNs with good aqueous stability. The peptide ($Peptide_1$) is encoded with an Arg-Gly-Asp (RGD) segment as the biorecognition element, which is able to target integrin receptors overexpressed in many tumor cells;[15] whereas, the RGD-free peptide ($Peptide_2$) is chosen as a control for comparison.

Results and Discussion

The synthetic route toward **P1** is shown in Scheme 2. 9,9-Bis(2-(2-(2-methoxyethoxy)ethoxy)ethyl)-2,7-divinylfluorene (**1**) was synthesized in 59% yield by heating a mixture of 2,7-dibromo-9,9-bis(2-(2-(2-methoxyethoxy)-ethoxy)ethyl)-fluorene and tributylvinyltin in toluene using $PdCl_2(PPh_3)_2$/2,6-di-*tert*-butylphenol as catalyst at 100 °C for 24 h. 2,7-Dibromo-9,9-bis(4-sulfonatobutyl)fluorene disodium (**2**) was synthesized in 60% yield by reacting 2,7-dibromofluorene with 1,4-butanesultone in a mixture of aqueous NaOH (50 wt %) and dimethyl sulfoxide (DMSO) in the presence of tetrabutylammonium bromide (TBAB).[16] Bromination of 2,1,3-benzothiadiazole in hydrobromic acid led to 4,7-dibromobenzothiadiazole (**3**).[17] Finally, a $Pd(OAc)_2$/P(*o*-tolyl)$_3$-catalyzed Heck condensation

(9) (a) Sigurdson, C. J.; Nilsson, K. P. R.; Hornemann, S.; Manco, G.; Polymenidou, M.; Schwarz, P.; Leclerc, M.; Hammarström, P.; Wüthrich, K.; Aguzzi, A. *Nat. Methods* **2007**, *4*, 1023–1030. (b) McRae, R. L.; Phillips, R. L.; Kim, I. B.; Bunz, U. H.; Fahmi, C. J. *J. Am. Chem. Soc.* **2008**, *130*, 7851–7853. (c) Pu, K. Y.; Li, K.; Shi, J.; Liu, B. *Chem. Mater.* **2009**, *21*, 3816–3822. (d) Feng, X.; Tang, Y.; Duan, X.; Liu, L.; Wang, S. *J. Mater. Chem.* **2010**, *20*, 1312–1316. (e) Pu, K. Y.; Li, K.; Liu, B. *Adv. Mater.* **2010**, *22*, 643–646. (f) Pu, K. Y.; Li, K.; Liu, B. *Adv. Funct. Mater.* **2010**, *20*, 2770–2777. (g) Pu, K. Y.; Li, K.; Zhang, X. H.; Liu, B. *Adv. Mater.* **2010**, *22*, 4186–4189.
(10) (a) Niidome, T.; Huang, L. *Gene Ther.* **2002**, *9*, 1647–1652. (b) Liu, Y. M.; Wenning, L.; Lynch, M.; Reineke, T. M. *J. Am. Chem. Soc.* **2004**, *126*, 7422–7423. (c) Putnam, D. *Nat. Mater.* **2006**, *5*, 439–451. (d) Husseini, G. A.; Pitt, W. G. *Adv. Drug Delivery Rev.* **2008**, *60*, 1137–1152.
(11) (a) Tan, C.; Pinto, M. R.; Kose, M. E.; Ghiviriga, I.; Schanze, K. S. *Adv. Mater.* **2004**, *16*, 1208–1212. (b) Liu, B.; Bazan, G. C. *J. Am. Chem. Soc.* **2006**, *128*, 1188–1196. (c) Pu, K. Y.; Fang, Z.; Liu, B. *Adv. Funct. Mater.* **2008**, *18*, 1321–1328. (d) Lee, K. W.; Cho, J. C.; DeHeck, J.; Kim, J. S. *Chem. Commun.* **2006**, 1983–1985.
(12) (a) Lakowicz, J. R. *Principles of Fluorescence Spectroscopy*, 3rd ed.; Springer, LLC: New York, 2006. (b) Fan, C. H.; Plaxco, K. W.; Heeger, A. J. *Trends Biotechnol.* **2005**, *23*, 186–192.
(13) (a) Schwartz, B. J. *Annu. Rev. Phys. Chem.* **2003**, *54*, 141–172. (b) Hennebicq, E.; Pourtois, G.; Scholes, G. D.; Herz, L. M.; Russell, D. M.; Silva, C.; Setayesh, S.; Grimsdale, A. C.; Müllen, K.; Brédas, J. L.; Beljonne, D. *J. Am. Soc. Chem.* **2005**, *127*, 4744–4762.
(14) (a) Liu, B.; Bazan, G. C. *J. Am. Chem. Soc.* **2004**, *126*, 1942–1943. (b) Pu, K. Y.; Liu, B. *Macromolecules* **2008**, *41*, 6636–6640. (c) Yu, D.; Zhang, Y.; Liu, B. *Macromolecules* **2008**, *41*, 4003–4011. (d) Dishari, S. K.; Pu, K. Y.; Liu, B. *Macromol. Rapid Commun.* **2009**, *30*, 1645–1650. (e) Shi, J. B.; Pu, K. Y.; Zhan, R. Y.; Liu, B. *Macromol. Chem. Phys.* **2009**, *210*, 1195–1200. (f) Shi, J. B.; Cai, L. P.; Pu, K. Y.; Liu, B. *Chem. Asian J.* **2010**, *5*, 301–308.
(15) (a) Ruoslahti, E. *Annu. Rev. Cell Dev. Biol.* **1996**, *12*, 697–715. (b) Nasongkla, N.; Shuai, X.; Ai, H.; Weinberg, B. D.; Pink, J.; Boothman, D. A.; Gao, J. *Angew. Chem., Int. Ed.* **2004**, *43*, 6323–6327.
(16) (a) Huang, F.; Wang, X.; Wang, D.; Yang, W.; Cao, Y. *Polymer* **2005**, *46*, 12010–12015. (b) Pu, K. Y.; Liu, B. *J. Phys. Chem. B* **2010**, *114*, 3077–3084.
(17) Liu, B.; Bazan, G. C. *Nat. Protoc.* **2006**, *1*, 1698–1702.

Scheme 2. Synthesis Route of P1[a]

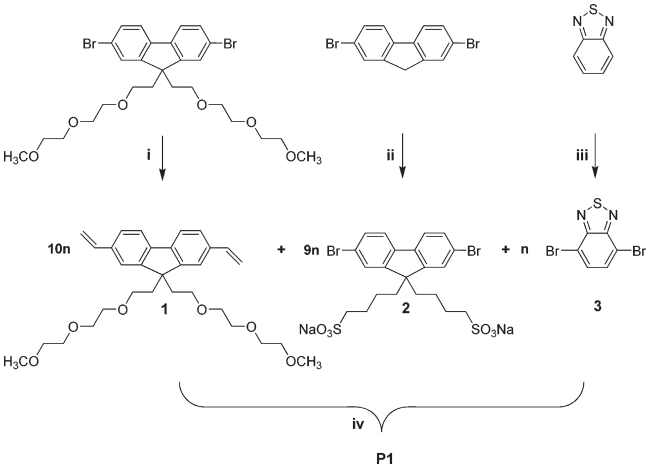

[a] Reagents and Conditions: (i) Tributylvinyltin, $PdCl_2(PPh_3)_2$/2,6-di-*tert*-butylphenol, toluene, 100 °C, 24 h; (ii) 1,4-butane sultone, TBAB, DMSO/NaOH aqueous solution, room temperature; (iii) Br_2, 48% HBr, reflux 3 h; (iv) $Pd(OAc)_2/P(o\text{-tolyl})_3$, DMF/$H_2O$/TEA, 100 °C, 12 h.

polymerization was conducted for **1**, **2**, and **3** at a molar ratio of 10:9:1 to directly afford the water-soluble anionic CPE (**P1**). The polymer is purified by microfiltration, precipitation, and finally dialysis against Mill-Q water using a 6.5 kDa molecular weight cutoff dialysis membrane. The molar ratio of BT in **P1** is estimated to be ~5 mol % according to the ^{1}H NMR spectrum shown in the Supporting Information as Figure S1.

Figure 1a shows the UV−vis absorption and photoluminescence (PL) spectra of **P1** in water. The polymer concentration is 4 μM based on repeat unit (RU).[18] It has an absorption maximum at 430 nm with a shoulder peak at 458 nm, both of which correspond to vinyl fluorene segments. The weak absorption band ranging from 500 to 550 nm arises from the small amount of BT units. The PL spectrum of **P1** in water is dominated by the donor emission of vinyl fluorene segments with a maximum at 472 nm, while the weak acceptor emission of BT units appears in the range of 575 to 700 nm. As such, the fluorescent color of **P1** aqueous solution is blue, indicating that self-aggregation is not severe for **P1** in water.[19] The PL quantum yield of **P1** in water is 17%, measured using quinine sulfate in 0.1 M H_2SO_4 (Φ = 0.55) as the standard.

To optimize the molar ratio of peptide to CPE for the formation of FNs with desirable optical properties, changes in the PL spectrum of **P1** (8 μM) in 25 mM phosphate-buffer saline (PBS, pH = 7.4) upon addition of $Peptide_1$ (0 to 1 μM) were monitored. As depicted in Figure 1b, the BT emission at 625 nm progressively grows at the expense of the vinyl-fluorene emission at 472 nm with increased [$Peptide_1$]. Accordingly, the fluorescent color of **P1** solution gradually changes from sky-blue to orange-red (Figure 1c),

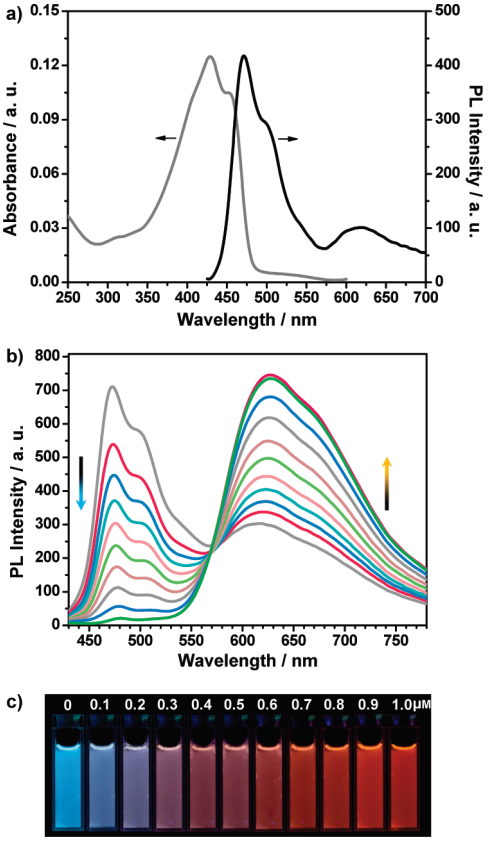

Figure 1. (a) UV−vis and PL spectra of **P1** ([RU] = 4 μM) in water. (b) PL spectra of **P1** ([RU] = 8 μM) in 15 PBS (pH = 7.4) upon addition of $Peptide_1$ with [Peptide1] ranging from 0 to 1 μM at intervals of 0.1 μM. (c) Photographs of the corresponding fluorescent solutions under UV radiation at 365 nm.

reflecting the gradually enhanced FRET from the vinyl fluorene segments (energy donor) to the BT units (energy acceptor). This enhancement stems from complexation-induced polymer aggregation because of the net positive charges possessed by the K segment of $Peptide_1$ at pH = 7.4. Within these aggregates, energy transfer dimensionality and electronic coupling between optical partners improve as compared to their separated states, ultimately leading to enhanced acceptor emission. The saturation occurs at [$Peptide_1$] = 0.90 μM, where the entire system has net negative charges left over from negatively charged **P1**. At this point, the PL quantum yield of **P1**/$Peptide_1$ complex is 16%, while the apparent Stokes shift significantly increases from 42 nm for **P1** itself to 195 nm for the FNs. As a result, variation of the molar ratio of **P1** to $Peptide_1$ in complex formation allows one to adjust the fluorescent color for cellular imaging.

The self-assembly properties of **P1**/$Peptide_1$ complexes at the molar ratios of 8:0.2 and 8:0.9 were examined by laser light scattering (LLS), where the complexes emit sky-blue, and orange-red fluorescence (Figure 1c), respectively. As depicted in Figure 2a, unimodal distribution peaks are observed for both complex solutions, revealing the formation of nanoparticles with diameters of 112 nm (8:0.2) and 205 nm (8:0.9), respectively. Further variation of the **P1** to Peptide1 molar ratio from 8:0.2 to 8:0.4 and 8:0.7 yielded pink and orange nanoparticles with diameters

(18) [RU] includes 0.5 mol OEO-substituted fluorene, 0.45 mol sulphate-substituted fluorene and 0.05 mol BT.

(19) (a) Wang, F.; Bazan, G. C. *J. Am. Chem. Soc.* **2006**, *128*, 15786–15792. (b) Satrijo, A.; Swager, T. M. *J. Am. Chem. Soc.* **2007**, *129*, 16020–16028. (c) Pu, K. Y.; Cai, L. P.; Liu, B. *Macromolecules* **2009**, *42*, 5933–5940. (d) Pu, K. Y.; Zhan, R. Y.; Liu, B. *Chem. Commun.* **2010**, *46*, 1470–1472.

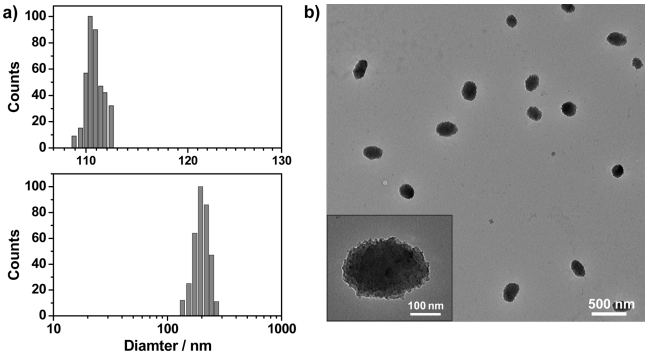

Figure 2. (a) Hydrodynamic radius distribution of **P1**/Peptide$_1$ complexes in PBS (15 mM, pH = 7.4) at [RU]/[Peptide$_1$] = 8: 0.2 (top) and [RU]/[Peptide$_1$] = 8: 0.9 (bottom) with [RU] = 8 μM. (b) The TEM image of **P1**/Peptide$_1$ complexes in dry state at [RU]/[Peptide$_1$] = 8: 0.9 with [RU] = 8 μM.

of 142 and 186 nm, respectively, by LLS measurement. It is also important to note that the scattering signal is hardly detectable for the solution of **P1** itself. Transmission electron microscopy (TEM) was further used to observe the morphology of **P1**/Peptide$_1$ complexes with the molar ratio of 8: 0.9 in dry state. As shown in Figure 2b, the assembled nanoparticles are elliptical with the major and minor axes of 250 and 185 nm, respectively. This nonspherical morphology should originate from particle collapse upon converting from solution state into dry state. It is also observable that the inner part of the nanoparticles is darker than the outer part (Inset of Figure 2b), manifesting a core−shell nanostructure. Considering the high electron density of the unsaturated π-conjugated backbone of **P1**, the inner core and outer shell of the nanoparticles should be enriched with **P1** and peptide, respectively. As RGD groups are neutral at pH = 7.4,[20] they should be located on the nanoparticle surface, consequently facilitating their specific interactions with integrin receptors in extracellular domain of tumor cells. These FNs are stable for days because of their net negative charges and the hydrophilic OEO side chains of **P1**. Moreover, changing Peptide$_1$ into Peptide$_2$ (a nonspecific RGD-free peptide in Scheme 1) resulted in FNs with nearly the same optical and morphological properties as those for the **P1**/Peptide$_1$ FNs. This similarity reflects the generality of complexation-mediated self-assembly strategy for the preparation of nanoparticles with varying size, components and fluorescence.

The effectiveness of the **P1**/Peptide$_1$ FNs in targeted cellular imaging was tested using HT29 cancer cells with overexpressed integrin receptors as an example. The molar ratio is chosen at 8: 0.9 considering the orange-red emission (625 nm) and the large Stokes shift (195 nm) of the corresponding FNs. The result was also compared with **P1** itself and the nonspecific **P1**/Peptide$_2$ FNs. After incubating the cells with the solution of the FNs or **P1** (1 μM based on RU) for 2 h at 37 °C, the cells were fixed and the nuclei were stained with 4′,6-diamidino-2-phenylindole (DAPI) for confocal laser scanning microscopy (CLSM) studies. The large Stokes shift of the FNs allows sample

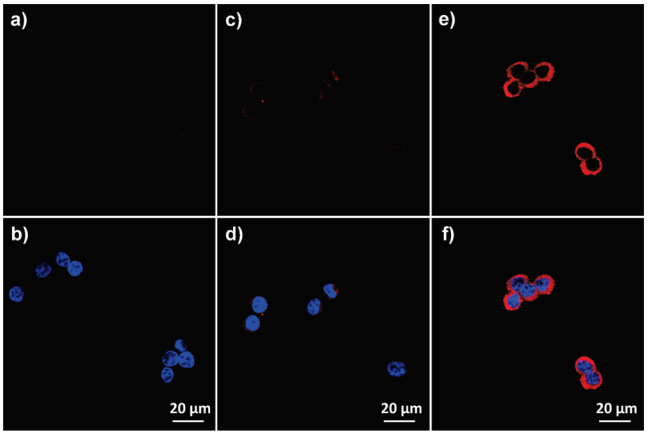

Figure 3. CLSM fluorescence and overlay images of HT29 cells incubated with **P1** (a and b), the **P1**/Peptide$_2$ FNs (c and d), and the **P1**/Peptide$_1$ FNs (e and f) for 2 h at 37 °C. The nuclei were stained by DAPI. [RU] = 1 μM and the molar ratio = 8:0.9. Excitation at 408 nm and collection of fluorescence signals from 575 to 635 nm.

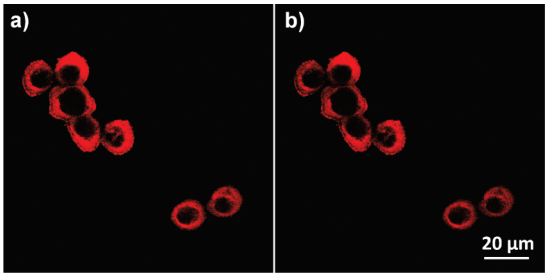

Figure 4. Time-resolved CLSM fluorescence images of HT29 cells stained by the **P1**/Peptide$_1$ FNs under continuous laser scanning for (a) 0 min and (b) 15 min. [RU] = 1 μM and the molar ratio = 8:0.9. Excitation at 408 nm and collection of fluorescence signals from 575 to 635 nm.

excitation at short wavelength (408 nm) while signal collection at long-wavelength range (575 to 635 nm), which is beneficial to minimizing the interference from cellular autofluorescence at high-energy region. As shown in Figures 3a-b, there is no visible fluorescence from the cells treated with **P1** itself, and there are only a few fluorescent dots for the cells treated with the **P1**/Peptide$_2$ FNs. The fluorescence is also invisible for **P1**-treated cells when collecting fluorescence signals from 455 to 495 nm. On the contrary, strong fluorescence from the cellular cytoplasm is observed for the cells treated with the **P1**/Peptide$_1$ FNs (Figures 3e-f). This implicates that these FNs are efficiently internalized by the cells and accumulated in the cytoplasm, which is promoted by the specific binding between RGD and integrin receptors in extracellular domains of HT29 cell.[21] A similar imaging pattern was also observed when the sky-blue **P1**/Peptide$_1$ FNs (8: 0.2) were used (Supporting Information, Figure S2). These data clearly demonstrate that the **P1**/Peptide$_1$ FNs with varying fluorescent colors can be utilized for molecular targeting.

To explore the potential of these complexes in long-term clinical applications, photostability of the orange-red **P1**/Peptide$_1$ FNs was evaluated. As shown in Figures 4a

(20) Müller, G.; Gurrath, M.; Kessler, H.; Timpl, R. *Angew. Chem., Int. Ed. Engl.* **1992**, *31*, 326–328.

(21) Wadih, A.; Pasqualini, R.; Ruoslahti, E. *Science* **1998**, *279*, 377–380.

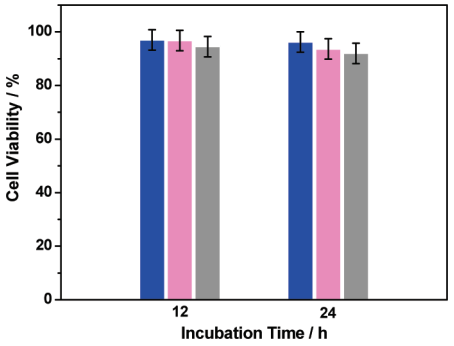

Figure 5. In-vitro viability of NIH-3T3 cells treated with **P1** solutions at the concentration of 1 (blue), 5 (pink), or 10 (gray) μM for 12 and 24 h, respectively. The percentage cell viability of treated cells is calculated relative to that of untreated cells with a viability arbitrarily defined as 100%.

and 4b, the fluorescent intensity decrease in the range of 575 to 635 nm is less than 10% after continuous laser scanning for 15 min. In comparison, most commercial dyes (such as fluorescein and rhodamine) usually lose their brightness after CLSM laser illumination for ~3 min.[9b] The sustained brightness in Figure 4b proves a relatively high photostability of the FNs in harsh physiological condition. Considering that **P1** constitutes the main component of the FNs, its cytotoxicity was also tested for mouse embryonic fibroblast cells (NIH-3T3) using an MTT cell-viability assay. As shown in Figure 5, the in vitro NIH-3T3 cell viability after being cultured with **P1** solutions at the concentration of 1, 5, or 10 μM for 12 or 24 is close to 100%, indicating low cytotoxicity of **P1**. These data prove that the **P1**/Peptide$_1$ FNs are highly desirable for practical imaging applications.

Conclusion

In conclusion, we have demonstrated a simple strategy to prepare multicolor CPE/peptide self-assembled FNs for receptor-targeted cellular imaging. The nanoparticle design takes advantage of efficient aggregation-enhanced energy transfer properties of CPEs in conjunction with electrostatic-interaction-induced aggregation to overcome the intrinsic drawbacks of chromophore-based FNs, endowing the FNs with extremely large Stokes shift (195 nm), good quantum yield in the long-wavelength region (16%), and good photostability. More importantly, the targeting capability is facilely in situ integrated into the CPE/peptide complexes through utilization of RGD terminated peptide. To the best of our knowledge, this is the first example of targeted imaging using label-free CPE. From the practical perspective, our CPE-based FN strategy can be generalized to fulfill various molecular imaging tasks simply by varying peptide into other biorecognition elements, such as antibodies, aptamers and small-molecule ligands. In addition, adjustment of the molar ratio between CPE and biorecognition element allows to fine-tune both fluorescent color and dimension of FNs for specific applications. This study thus not only brings label-free conjugated polymers into targeted molecular imaging, but also provides a new concept to construct polymeric FNs with controllable features for biological applications.

Experimental Section

Instruments. NMR spectra were collected on Bruker Avance 500 (DRX 500, 500 MHz). Matrix-assisted laser desorption/ionization time-of-flight (MALDI-TOF) was performed by using 2,5-dihydroxybenzoic acid (DHB) as the matrix under the reflector mode for data acquisition. UV−vis spectra were recorded on a Shimadzu UV-1700 spectrometer. PL measurements were carried out on a Perkin-Elmer LS-55 equipped with a xenon lamp excitation source and a Hamamatsu (Japan) 928 PMT, using 90 degree angle detection for solution samples. Photographs of the polymer solutions were taken using a Canon EOS 500D Digital camera under a hand-held UV-lamp with $\lambda_{max} = 365$ nm. Fisher brand regenerated cellulose dialysis tubing with 6.5 kDa molecular weight cutoff was used for polymer dialysis. Freeze-drying was performed using Martin Christ Model Alpha 1−2/LD. LLS measurements were performed using Brookhaven Instruments Corporation (BIC) 90 Plus with $\lambda = 659$ nm, and the particle diameters were calculated by ZetaPlus Particle Sizing Software Version 3.93. TEM images were obtained from a JEOL JEM-2010 transmission electron microscope with an accelerating voltage of 200 kV. All UV and PL spectra were collected at 24 ± 1 °C. Milli-Q water (18.2 MΩ) was used for all the experiments.

Materials. The peptides (KKKKKKKRGD and KKKKKKKKK) were purchased from first BASE Singapore. Fetal bovine serum (FBS) was purchased from Gibco (Lige Technologies, Ag, Switzerland). 3-(4,5-Dimethylthiazol-2-yl)-2,5-diphenyl tetrazolium bromide (MTT) and penicillin-streptomycin solution were purchased from Sigma-Aldrich. Dulbecco's modified essential medium (DMEM) was a commercial product of National University Medical Institutes (Singapore). Ten × phosphate-buffer saline (PBS) buffer with pH = 7.4 (ultrapure grade) is a commercial product of first BASE Singapore. Milli-Q water (18.2 MΩ) was used to prepare the buffer solutions from the 10 × PBS stock buffer. NMR solvents, D_3-chloroform (99%), D_6-DMSO (99.5%), and D_4-methanol (99.5%) were purchased from Cambridge Isotope Laboratories, Inc. 2,7-Dibromo-9,9-bis(2-(2-(2-methoxyethoxy)ethoxy)ethyl)-fluorene and 4,7-dibromobenzothiadiazole (**3**) were synthesized according to our previous report.[17]

Cell Cultures. HT29 tumor cells and NIH-3T3 fibroblast were cultured in DMEM containing 10% fetal bovine serum and 1% penicillin streptomycin at 37 °C in a humidified environment containing 5% CO_2. Before experiment, the cells were precultured until confluence was reached.

Confocal Imaging. HT29 cells were cultured in the chambers (LAB-TEK, Chambered Coverglass System) at 37 °C for a qualitative study. After 80% confluence, the medium was removed, and the adherent cells were washed twice with 1 × PBS buffer. The FNs solution (1 μM base on RU, 0.8 mL) was then added to the chamber. After incubation for 1 h, cells were washed three times with 1 × PBS buffer and then fixed by 75% ethanol for 20 min and further washed twice with 1 × PBS buffer. The nuclei were stained with DAPI for 30 min. The cell monolayer was washed twice with 1 × PBS buffer and imaged by CLSM, Zeiss LSM 410, Jena, Germany with imaging software Fluoview FV500.

Cytotoxicity Test. MTT assays were performed to assess the metabolic activity of NIH-3T3 fibroblast. NIH-3T3 cells were seeded in 96-well plates (Costar, IL, U.S.A.) at an intensity of 2×10^4 cells/mL. After 48 h incubation, the medium was replaced by **P1** solution at the concentration of 1, 5, or 10 μM, and the cells were then incubated for 12 and 24 h, respectively. After the designated time intervals, the wells were washed twice with

1 × PBS buffer and freshly prepared MTT (100 μL, 0.5 mg/mL) solution in culture medium was added into each well. The MTT medium solution was carefully removed after 3 h incubation in the incubator. Isopropanol (100 μL) was then added into each well and gently shaken for 10 min at room temperature to dissolve all the precipitate formed. The absorbance of MTT at 570 nm was monitored by the microplate reader (Genios Tecan). Cell viability was expressed by the ratio of the absorbance of the cells incubated with **P1** solution to that of the cells incubated with culture medium only.

Synthesis of 9,9-Bis(2-(2-(2-methoxyethoxy)ethoxy)ethyl)-2,7-divinylfluorene (1). 2,7-Dibromo-9,9-bis(2-(2-(2-methoxyethoxy)-ethoxy)ethyl)-fluorene (1.23 g, 2.0 mmol), tributylvinyltin (1.33 g, 4.2 mmol), $PdCl_2(PPh_3)_2$ (56 mg, 0.09 mmol), and 2,6-di-*tert*-butylphenol (8 mg, 38 mmol), and toluene (20 mL) were mixed in a 50 mL flask. The reaction mixture was stirred and heated at 100 °C for 24 h under N_2. After cooling to the room temperature, the mixture was diluted with ether and treated with KF solution(∼ 10%), which was followed by stirring for 12 h. The mixed solution was then filtrated to remove the insoluble solid, and the filtrate was dried over anhydrous Na_2SO_4. The solvent was removed under reduced pressure, and the residue was chromatographed on silica gel using hexane/ethyl acetate (1:1) as eluent to give **1** (0.70 g, 68%) as a nattierblue liquid. ^{1}H NMR (500 MHz, $CDCl_3$, δ ppm): 7.60 (d, 2 H, J = 7.8 Hz), 7.44 (s, 2 H), 7.39 (d, 2 H, J = 7.7 Hz), 6.78 (dd, 2 H, J = 10.9, 17.6 Hz), 5.80 (d, 2 H, J = 17.5 Hz), 5.27 (d, 2 H, J = 10.9 Hz), 3.51 (dd, 4 H, J = 3.4, 5.9 Hz), 3.46 (dd, 4 H, J = 3.3, 6.0 Hz), 3.39 (t, 4 H, J = 3.2 Hz), 3.33 (s, 6 H), 3.21 (t, 4 H, J = 3.3 Hz), 2.76 (t, 4 H, J = 5 Hz), 2.40 (t, 4 H, J = 5.17 Hz). ^{13}C NMR (125 MHz, $CDCl_3$, δ ppm): 149.50, 139.96, 137.00, 136.83, 125.82, 120.69, 119.85, 113.54, 71.83, 70.43, 70.39, 69.96, 66.98, 58.96, 50.96, 39.75. MS (MALDI-TOF): m/z 510.27 [M^+].

Synthesis of 2,7-Dibromo-9,9-bis(4-sulfonatobutyl)fluorene disodium (2). 2,7-Dibromofluorene (4 g, 12 mmol) and tetrabutylammoium bromide (80 mg) were dissolved in the mixture of a 50 wt % aqueous solution of sodium hydroxide (8 mL) and DMSO (60 mL). A solution of 1,4-butane sultone (4 g, 29 mmol) in DMSO (20 mL) was dropwise added into the mixture under nitrogen. After being stirred at room temperature for 4 h, the reaction mixture was precipitated into acetone to afford the crude product. The product was collected by filtration, washed with ethanol, recrystallized twice from acetone/H_2O, and dried under vacuum at 60 °C for 24 h to yield (**2**) as white needle crystals (4.3 g, 58.6%). ^{1}H NMR (500 MHz, CD_3OD, δ ppm): 7.68 (d, 2 H, J = 8.11 Hz), 7.63 (d, 2 H, J = 1.45 Hz), 7.52 (dd, 2 H, J = 1.42, 8.08 Hz), 2.68−2.47 (m, 4 H), 2.22−2.00 (m, 4 H), 1.62 (td, 4 H, J = 7.83, 7.83, 15.65 Hz,), 0.67 (td, 4 H, J = 7.83, 7.83, 15.65 Hz). ^{13}C NMR (125 MHz, CD_3OD, δ ppm): 153.39, 140.68, 131.61, 127.38, 122.74, 122.52, 52.37, 40.76, 26.19, 24.25. MS (MALDI-TOF): m/z 619.89 [M − Na]$^-$.

Synthesis of P1. 1 (216 mg, 0.423 mmol), **2** (244 mg, 0.380 mmol), **3** (12.5 mg, 0.043 mmoL), $Pd(OAc)_2$ (4.0 mg, 0.018 mmol), and P(*o*-tolyl)$_3$ (30 mg, 0.098 mmol) were placed in a 25 mL round-bottom flask. A mixture of DMF (4.0 mL), H_2O (1.0 mL), and triethylamine (1.5 mL) was added to the flask, and the reaction vessel was degassed. The mixture was vigorously stirred at 105 °C for 12 h. It was then filtered, and the filtrate was poured into acetone. The precipitate was collected and washed to afford red powders. The crude product was dissolved in methanol and further purified by dialysis against Mill-Q water using a 6.5 kDa molecular weight cutoff dialysis membrane for 5 days. After freeze-drying, **P1** (315 mg, 72%) was obtained as red fibers. ^{1}H NMR (500 MHz, d_6-DMSO, δ ppm): 8.35−6.88 (m, 15.8 H), 3.56 (br, 12), 3.43−3.21 (m, 7.8), 2.74 (br, 12 H), 2.41−1.79 (m, 7.8), 1.43 (br, 3.8), 0.60 (br, 3.8). ^{13}C NMR (125 MHz, d_6-DMSO, δ ppm): 154.02, 152.81, 151.38, 150.26, 140.48, 139.70, 139.24, 137.09, 133.09, 132.52, 130.55, 128.91, 126.55, 126.22, 121.31, 120.74, 71.67, 70.16, 70.00, 69.84, 58.45, 54.94, 51.82, 51.26, 46.19, 29.48, 25.84, 23.52.

Acknowledgment. The authors are grateful to the National University of Singapore (R-279-000-234-123, R279-000-301-646), Singapore Ministry of Education (R-279-000-255-112), and Ministry of Defense (R-279-000-301-232) for financial support.

Supporting Information Available: The NMR spectrum of **P1** and the CLSM images of the sky-blue FNs are given in Figures S1 and S2. This material is available free of charge via the Internet at http://pubs.acs.org.